JOURNAL OF COASTAL AND HYDRAULIC STRUCTURES

Vol. 1, 2021, 7

Optimum Layouts of a Cluster of Five Heaving Point Absorbers in front of Wall-type Coastal Structures under Perpendicular Regular Wave Attack

Rafail Ioannou[1] and Eva Loukogeorgaki [2]

Abstract

The present paper aims at determining optimum layouts for a cluster of identical semi-immersed oblate spheroidal heaving Point Absorbers (PAs) in front of a bottom-mounted wall-type structure under the action of regular waves. Optimum layouts correspond to those that for a given incident wave frequency and direction maximize the power absorbed by the cluster and satisfy predefined spatial constraints. The corresponding optimization problem is solved by developing and coupling a Genetic Algorithm (GA) solver with a frequency-based hydrodynamic analysis numerical model. Initially, the efficiency of the developed optimization process is assessed by comparing results with the parametric ones of other investigators. Next, various optimization cases for a cluster of five devices under the action of incident waves perpendicular to the wall are formed and solved. Focus is given on the effect of two different incident wave frequencies, the available wall length for deploying the devices and of symmetrical layout considerations, on the formation of the optimum layouts and on the power absorbed by the cluster.

When optimization is performed at a frequency smaller than the heave natural frequency of the devices, the PAs within the optimum layouts are placed close to the wall and they form sub-clusters of closely-positioned bodies. Contrary to the above, maximization of the absorbed power at a frequency equal to the devices' heave natural frequency is realized by placing the PAs at a large perpendicular distance from the wall and without forming any sub-clusters. In the latter case, the optimally-arranged devices show also a much better power absorption ability. The deployment of part of the whole wall length for placing the PAs reduces the power absorbed by the optimally-arranged clusters, compared to the cases, where no wall-length restrictions are taken into account. Finally, the consideration of symmetrical features in the formation of the optimum layouts reduces at a small degree the power absorption ability of the PAs clusters.

Keywords

Wave energy, Point absorbers, Cluster, Vertical wall, Layout, Optimization, Genetic Algorithm

[1]ikrafail@civil.auth.gr, Aristotle University of Thessaloniki, Thessaloniki, Greece
[2]eloukog@civil.auth.gr, Aristotle University of Thessaloniki, Thessaloniki, Greece

This paper was submitted on July 23, 2021. It was accepted after double-blind review on 9 November 2021 and published online on 24 November 2021.

DOI: https://doi.org/10.48438/jchs.2021.0007

Cite as: "Ioannou, R., & Loukogeorgaki, E. (2021). Optimum layouts of a cluster of five heaving point absorbers in front of wall-type coastal structures under perpendicular regular wave attack, 1. https://doi.org/10.48438/jchs.2021.0007"

1 Introduction

Energy is fundamental for the evolution and the sustainability of modern societies. Renewable energy sources have already been established as the future of energy production, since the overexploitation of current mineral sources reserves is predicted to lead not only to their exhaustion over the forthcoming decades, but, also, to high cumulative CO_2 emissions and global temperatures (Exxon Mobil Corporation 2019; Raftery et al. 2017). Wave energy stands out among the various renewable energy resources, as an innovative alternative to meet the future energy demands. Accordingly, a variety of Wave Energy Converters (WECs) has been developed over the years (e.g. López et al. 2013; Rusu and Onea 2018), by continuously advancing the relevant technology. However, the wave energy sector is still characterized by a high levelized cost of energy (Astariz et al. 2015; Rusu and Onea 2018) and, thus, there are challenges that have to be overcome in order to deliver cost-competitive commercial solutions. Among the various WEC types developed so far, Point Absorbers (PAs) correspond to the most technologically advanced devices (López et al. 2013), that harvest the incoming wave energy usually through their oscillation along their vertical working direction.

For exploiting the vast wave energy resource in an extensive and cost-efficient manner, PAs either in offshore or near-shore sites have to be deployed in the form multi-body clusters. At near-shore locations, PAs clusters may be combined with existing coastal structures, such as vertical (wall-type) breakwaters, facilitating cost reduction. In those cases, hydrodynamic interactions between the vertical barrier and the PAs are introduced, which can improve the cluster's power absorption ability (e.g. Loukogeorgaki and Chatjigeorgiou, 2019; Loukogeorgaki et al. 2020). It is evident, however, that this improvement depends strongly upon the location of the PAs with respect to the wall and within the cluster. Hence, optimizing the layout of the cluster is a key factor towards the efficient utilization of PAs in the seaward side of vertical-front coastal structures.

Up to now, various researchers have demonstrated parametrically the significance of the layout characteristics of a PAs cluster in front of a bottom-mounted vertical wall on its performance (hydrodynamic behavior and power absorption) by conducting a relevant hydrodynamic analysis in the frequency domain. More specifically, Loukogeorgaki and Chatjigeorgiou (2019) and Loukogeorgaki et al. (2020) investigated the performance of a linear array of nine equally-spaced cylindrical and five oblate spheroidal, respectively, heaving PAs in front of a finite-length bottom-mounted wall and illustrated the direct effect of the devices-wall distance on the array's power absorption ability. By assuming a leeward wall of infinite length, Konispoliatis and Mavrakos (2020) considered a linear, parallel or perpendicular to the wall, array as well as a rectangular cluster of five equally-spaced cylindrical heaving PAs and studied the effect of the cluster-wall distance, the inter-body spacing and the cluster's shape on the performance of the cluster. The results illustrated that the cluster-wall distance significantly affects the power absorption ability of the devices, while this does not hold true for the inter-body spacing. Furthermore, the linear array situated parallel to the wall corresponded to the most power-efficient cluster configuration. The strong effect of the cluster's shape (linear, parallel to the wall array, linear, perpendicular to the wall, array and rectangular cluster) on the hydrodynamic characteristics of a PAs cluster has been also demonstrated by Konispoliatis et al. (2020) for the case of five heaving PAs with cylindrical, conical or semi-spherical floaters situated in front of a "pure" wave reflecting wall of infinite extent.

Regarding the determination of optimally-arranged clusters of various WEC types, the relevant problem has been tackled extensively by many researchers for isolated (i.e., without the wall presence) clusters. Accordingly, a variety of optimization techniques has been developed and deployed corresponding to: (a) traditional non-linear optimization techniques, such as the sequential quadratic programming method (e.g. McGuinness and Thomas 2016), (b) metaheuristic algorithms, including the Genetic Algorithm (GA) (e.g. Child and Venugopal 2010; Ruiz et al. 2017; Giassi and Göteman 2018; Sharp and DuPont 2018), the differential evolution algorithm (e.g. Fang et al. 2018) the covariance matrix adaptation strategy (e.g. Ruiz et al. 2017), the particle swarm algorithm (e.g. Ruiz et al. 2017) and the parabolic intersection method (e.g. Child and Venugopal 2010) as well as (c) advanced techniques, such as artificial neural networks (Neshat et al. 2019). A first research effort towards the layout optimization of a heaving PAs cluster in the presence of a vertical wall has been realized very recently in Loukogeorgaki et al. (2021), who developed a GA-based optimization framework to determine optimally-arranged clusters for real sea states (i.e., under the action of irregular waves). The framework was applied at specific near-shore locations in Greece, where the peak frequencies of the most dominant sea states were smaller than the heave natural frequency of the devices (equal to 2.4 rad/s). Accordingly, optimum layouts were determined for wave environments characterized by low peak frequencies (<2.0 rad/s).

In the present paper, we determine optimum layouts of a cluster of heaving PAs situated in front of a bottom-mounted finite-length vertical wall under the action of regular waves. The cluster consists of identical semi-immersed oblate spheroidal devices, while optimum layouts correspond to those that for a given incident wave frequency and direction maximize the averaged power absorbed by the cluster and satisfy simultaneously specific spatial constraints. The examined constrained optimization problem is solved by developing and coupling a GA solver with a frequency-based hydrodynamic analysis numerical model, which solves the diffraction/radiation problem of the multi-body arrangement in front of the wall by utilizing the conventional Boundary Integral Equation (BIE) method. The efficiency of the developed algorithm is, initially, assessed by comparing its results with the parametric ones of Loukogeorgaki et al. (2020) for the case of a linear PA array. Next, various optimization cases are formed and solved, aiming at investigating the effect of low and high incident wave frequencies and of the available for deploying the devices wall length on the formation of the optimum layouts and on the power absorbed by the cluster. Finally, symmetrical (with respect to the median of the wall) optimum layouts are determined and the effect of these symmetrical considerations on the power absorption ability of the optimally-arranged clusters is illustrated and discussed.

2 Methodology

2.1 General Problem's Definition

A cluster of N identical PAs is situated in front of a bottom-mounted vertical wall of finite length L_{wall} and of negligible thickness in an area of constant water depth d (Figure 1). The PAs correspond to semi-immersed, oblate spheroidal devices of radius α and draft c. Each PA$_i$, $i = 1, \dots, N$, is assumed to undergo small-amplitude oscillations only along its working direction, namely, along the local oz_i vertical axis (Figure 1(b)). Power absorption is realized via an axisymmetric linear Power Take-Off (PTO) mechanism, schematically represented in Figure 1(b) as a linear damping system of damping coefficient b_{PTOi}, $i = 1, \dots, N$. The PAs are distributed randomly in front of the wall, with X_i and Y_i, $i = 1, \dots, N$, denoting the $X$and Yspatial coordinates of the PAs centers in the global $OXYZ$ coordinate system, as shown in Figure 1(a). In this figure, L_{edge} is defined as the horizontal, along the global OX axis, distance of the two outer PAs from the two wall edges. The multi-body arrangement in front of the wall is subjected to the action of regular waves of unit amplitude and frequency ω, propagating at an angle β with respect to the OX axis (Figure 1(a)).

Based on the above, we seek to determine the optimum values of the PAs spatial coordinates that maximize the total averaged power absorbed by the cluster, p_{tot}, for a given incident wave frequency and direction, and satisfy simultaneously specific spatial constraints. Hence, the examined constrained optimization problem is mathematically formed as:

$$\text{maximize } p_{tot}(X_1, Y_1, \dots, X_i, Y_i, \dots, X_N, Y_N | \omega, \beta) \tag{1}$$

subjected to:

$$\sqrt{\left(X_i - X_j\right)^2 + \left(Y_i - Y_j\right)^2} > 2\alpha \text{ for } i, j = 1, \dots, N \text{ and } i \neq j \tag{2}$$

$$1.1\alpha \leq Y_i \leq 4\alpha \text{ for } i = 1, \dots, N \tag{3}$$

$$|X_i| \leq \frac{L_{wall}}{2} - L_{edge} \text{ for } i = 1, \dots, N \tag{4}$$

In Eq. 1, p_{tot} corresponds to the objective function, X_i and Y_i, $i = 1, \dots, N$, present the design variables that have to be optimized, while the symbol "|" is used to denote given values of ω and β. Regarding Eqs. 2-4, these equations express mathematically various spatial constraints. More specifically, Eq. 2 ensures avoidance of overlapping between any two devices, whereas Eq. 3 imposes limitations on the perpendicular distances of the PAs from the wall. The lower bound of Eq. 3 ensures avoidance of contact between a PA and the wall and the upper bound guarantees the sitting of the devices within an adequate distance from the bottom-mounted structure. It is noted that in the present investigation, nonlinear and viscous effects are neglected and, thus, minimum distances between the devices (Eq. 2) as well as between the PAs and the wall (Eq. 3) are defined considering only the requirement of overlapping avoidance. Finally, Eq. 4 ensures the

placement of all the devices in front of the wall. If $L_{edge} \neq 0$ m, the PAs are restrained to be distributed along part of the whole wall length, L_{wall}, while if $L_{edge} = 0$ m, the devices are free to be situated along the whole wall length. It is noted that if the formation of symmetrical (with respect to the global OY axis) layouts is being sought, the following constraints are additionally introduced:

$$\text{For odd } N \text{ number of PAs: } \begin{cases} X_i = -X_{N+1-i}, & \text{for } i = 1, \dots, (N/2 - 0.5) \\ X_{(N/2)+0.5} = 0 & \\ Y_i = Y_{N+1-i} & \text{for } i = 1, \dots, (N/2 - 0.5) \end{cases} \quad (5)$$

or

$$\text{For even } N \text{ number of PAs: } \begin{cases} X_i = -X_{N+1-i}, & \text{for } i = 1, \dots, N/2 \\ Y_i = Y_{N+1-i}, & \text{for } i = 1, \dots, N/2 \end{cases} \quad (6)$$

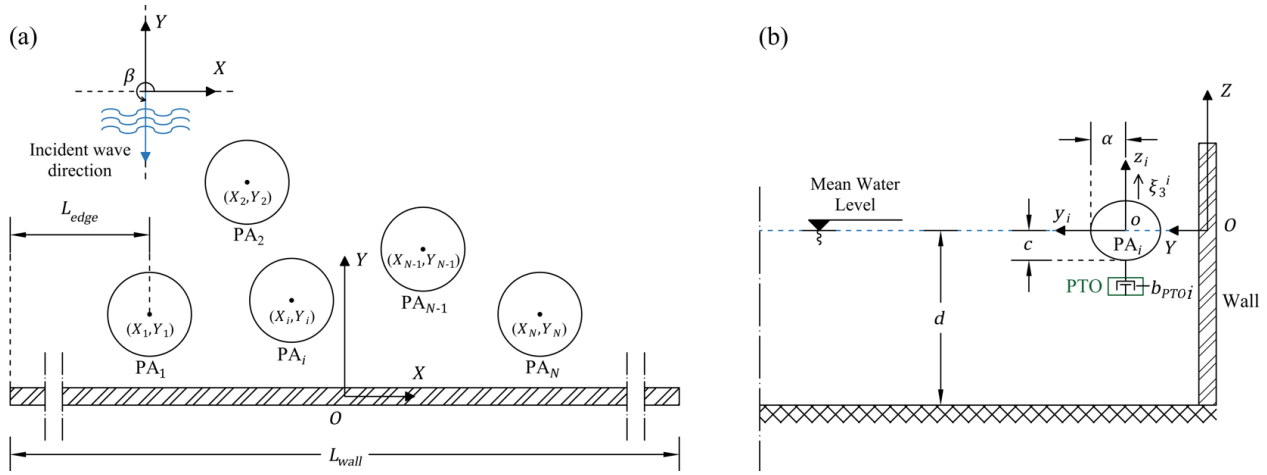

Figure 1 (a): Top view of the examined PAs cluster, (b): YZ cut plane view of a PA geometry in front of the vertical wall.

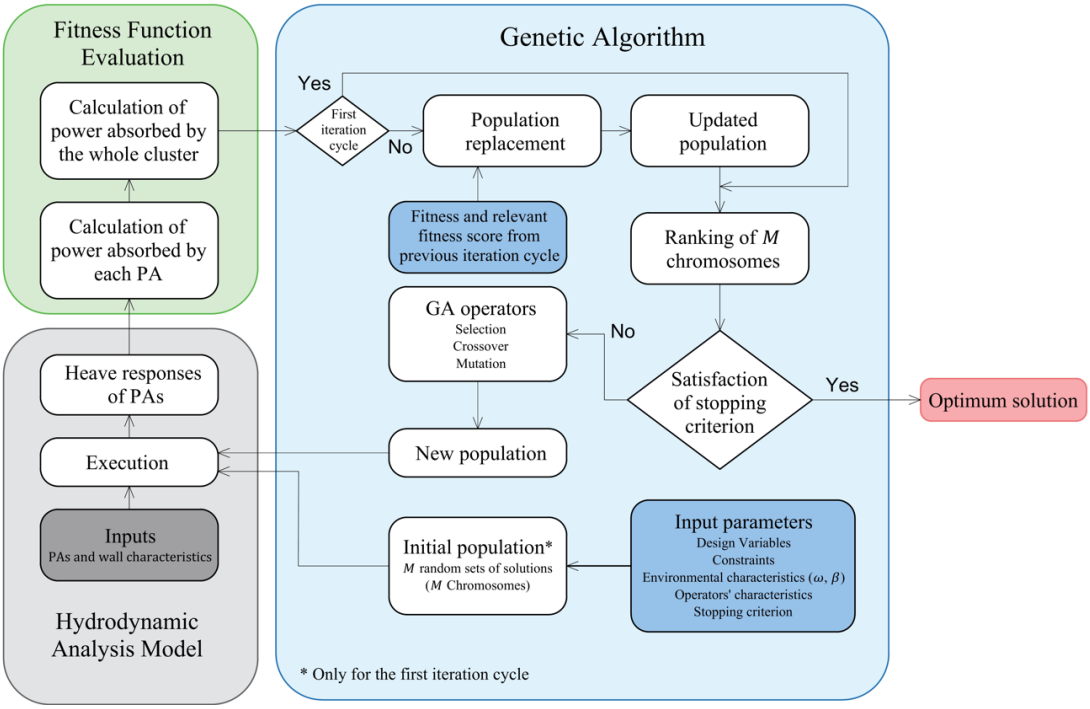

Figure 2 Coupling process of the GA code with the hydrodynamic analysis model for solving the examined constrained optimization problem.

In order to solve constrained optimization problem described above, a Genetic Algorithm (GA) code is developed from scratch and it is appropriately coupled with a frequency-based hydrodynamic analysis model (i.e., WAMIT ©, Lee 1995). The latter model solves the diffraction/radiation problem of the examined multi-body arrangement in the presence of the wall and enables the quantification of the objective function (Eq. 1). The relevant coupling process is shown schematically in Figure 2, while details about the two aforementioned numerical components are cited in the following sub-sections. The GA code and the coupling process were developed using MATLAB R2019a (The MathWorks, Inc. 2019).

2.2 Genetic Algorithm

A GA corresponds to a search evolutionary optimization method inspired by the process of biological evolution (Kumar et al. 2007). Within this context, a group of M candidate solutions (i.e., a population of M chromosomes) is evolving in time through a sequence of iteration cycles (generations). Each candidate solution (chromosome) consists of a set of values of the design variables, known as genes. The evolution is realized according to the "survival of the fittest" rule, where the fittest chromosomes are considered for reproduction in the subsequent generation. At each iteration, the ability of each chromosome to solve the optimization problem is quantified by calculating its fitness score (fitness function value), while reproduction is numerically realized by utilizing specific GA operators (i.e., ranking, selection, crossover and mutation). For the optimization problem examined in the present paper, a chromosome of a population consists of $2N$ genes, corresponding to a specific set of values of the design variables X_i and Y_i, $i = 1, \dots, N$, while the size of the population (i.e., number of candidate solutions), M, remains constant throughout the whole optimization process. Finally, the fitness function corresponds to the total power absorbed by the cluster, p_{tot}.

The optimization algorithm begins (1st iteration cycle) by generating a random, constraint dependent, initial population (Figure 2). Each chromosome (i.e., a candidate set of X_i and Y_i, $i = 1, \dots, N$, values) of this population is, then, used as input in the hydrodynamic analysis model in order to calculate the responses of the PAs and, thus, quantify the objective function p_{tot}. Next, ranking of the chromosomes of the initial population is performed in ascending order according to their fitness score, and the stopping criterion, related to a maximum number of predefined iteration cycles, is checked. If this criterion is not satisfied, a new population is generated by deploying successively the selection, the crossover and the mutation operators. It is noted that the convergence of the objective function to a certain value was not deployed in the present investigation as a stopping criterion, since for the characteristics of the problem examined it had led to an early convergence of the optimization algorithm to sub-optimum solutions.

The selection operator aims at selecting the fittest chromosomes (i.e., the fittest sets of X_i and Y_i, $i = 1, \dots, N$, values) as "parents" to pass their genes (i.e., the corresponding X_i and Y_i, $i = 1, \dots, N$, values) to the new population. The relevant selection technique utilized herein is based on the roulette wheel technique, where each chromosome corresponds to a sector of a roulette wheel with a central angle proportional to its selection probability (e.g., Razali and Geraghty 2011). Each time the wheel turns (i.e., generation of a random number at $[0, 1]$) a parent is selected. The parents are arranged in pairs, while the operator prevents the selection of the same parent in a pair. However, the same chromosome can be selected as a parent in multiple pairs. Considering that in the traditional roulette wheel technique the selection probability is calculated as the ratio of a chromosome's fitness score to the sum of the fitness scores of the whole population, the chance of a small sector being selected is very low (Haq et al. 2019). In order to overcome this drawback and, thus, avoiding a premature convergence of the optimization algorithm to a local maxima, the selection probability, PS_m, of an m^{th}, $m = 1, \dots, M$, chromosome is quantified according to the principles of the linear ranking selection scheme as follows (Davis 1991):

$$PS_m = \frac{\alpha_{sel} + \left[\frac{rank_m}{M-1}\right](\beta_{sel} - \alpha_{sel})}{M} \text{ for } m = 1, \dots, M \tag{7}$$

In Eq. (7), $rank_m$ is the rank value of the m^{th} chromosome within the population based on the ranking already implemented. This value is set equal to zero for the first in the ranking chromosome (i.e., the chromosome with the worst fitness score), while a rank value equal to $(M - 1)$ is assigned to the last in the ranking chromosome (i.e., the chromosome with the beset fitness score). The rank values (integer numbers) for the remaining chromosomes are defined within the aforementioned lower and upper bounds based on the chromosomes' relevant ranking positions. As for the rest variables

of Eq. (7), β_{sel} ($1.0 \leq \beta_{sel} \leq 2.0$) is the selective pressure representing the expected number of offsprings derived from the "best" parent, while α_{sel}, equal to $2.0 - \beta_{sel}$, refers to the parent with the worst fitness score. When β_{sel} is equal to 1.0, all chromosomes have equal selection probability, while as the β_{sel} value increases from 1.0 to 2.0, the selection probability of the best chromosomes becomes larger. It is noted that the utilization of Eq. (7) enables the selection of parents taking into account both the fitness score of the chromosomes and their diversity.

Having selected the "parents", new chromosomes (i.e., new sets of X_i and Y_i, $i = 1, \dots, N$, values) are generated by: (a) combining the genes of each pair of "parents" to reproduce a fitter offspring (crossover GA operator) and (b) changing randomly the genes of a single "parent", so that diversity within the population is maintained, while premature convergence is prevented (mutation GA operator). Regarding item (a), the uniform crossover technique is deployed with uniformly distributed genes from each "parent" (Gwiazda 2006). The allowable crossover rate, which is given as input to the algorithm, can take any constant value between 80% and 95%. As for item (b), a non-uniform mutation is implemented (Shopova and Vaklieva-Bancheva 2006), where genes undergo the process of dynamic real representation (Oyama et al. 2000). The allowable mutation rate, which is also provided as input to the algorithm, can take any constant value between 0% and 30%.

The chromosomes of the new population (i.e., new sets of X_i and Y_i, $i = 1, \dots, N$, values) are then used as input in the hydrodynamic analysis model starting the 2nd iteration cycle of the optimization algorithm. Accordingly, new values of p_{tot} are calculated. At this stage and prior performing ranking, a population replacement strategy is deployed (Figure 2). Within this context, the chromosomes of both the current (2nd iteration cycle) and the previous (1st iteration cycle) populations are "placed" in a sampling pool. Among the $2M$ chromosomes of the pool, the chromosome with the best fitness score is considered as "elite" and is included in the updated population, while the rest $(M - 1)$ chromosomes of the updated population are selected randomly from the remaining $(2M - 1)$ chromosomes of the pool. The aforementioned population replacement strategy is implemented at each subsequent iteration cycle until the termination of the algorithm. Having defined the updated population, its chromosomes are ranked and the stopping criterion is checked. If the stopping criterion is not satisfied (i.e., the current iteration cycle is smaller than the maximum allowable number of iteration cycles), the algorithm continues with the reproduction and the generation of a new population. If the opposite holds true, the algorithm is terminated and the chromosome of the last updated population having the best fitness score is assigned as the optimum solution of the examined optimization problem.

2.3 Hydrodynamic Analysis Model

In order to quantify the objective function p_{tot} (Eq. 1), hydrodynamic analysis of the examined PAs cluster in the presence of the wall, taking also into account the hydrodynamic interactions among all co-located bodies, is required. This analysis is implemented in the frequency domain and it relies on the BIE method, which is numerically realized using WAMIT© (Lee 1995). A three-dimensional linear diffraction theory is deployed, where the wall is considered fixed at its position, while the devices are taken to perform small-amplitude oscillations in the vertical direction (Figure 1(b)). Thus, for each PA$_i$, $i = 1, \dots, N$, all degrees of freedom, except the one corresponding to heave, are considered ideally restricted. The latter assumption can be physically realized by attaching the PAs on the wall via appropriate attachment configurations, which allow the devices to move only along the vertical direction (see for example Gkaraklova et al. 2021). Assuming inviscid and incompressible fluid with irrotational flow, the fluid motion is described by introducing the velocity potential. Its complex spatial part is defined as (Lee 1995; Lee and Newman 2005):

$$\varphi = \underbrace{(\varphi_I + \varphi_S)}_{\varphi_D} + i\omega \sum_{i=1}^{N} \xi_3^i \varphi_i \tag{8}$$

$$\varphi_I = \frac{igA}{\omega} \frac{cosh[k(Z+d)]}{cosh(kd)} e^{-ik(Xcos\beta + Ysin\beta)} \tag{9}$$

In the above equations, φ_I is the incident wave potential, φ_S is the scattered potential, associated with the disturbance of the incident waves induced by the PAs and the wall fixed at their positions, φ_D denotes the diffraction potential and φ_i, $i = 1, \dots, N$, are the radiation potentials, related to the waves radiated from the PAs due to their forced unit-amplitude motion in heave. Furthermore, ξ_3^i, $i = 1, \dots, N$, denote the complex amplitudes of the heave motions of the devices, g is the gravitational acceleration, A is the wave amplitude, k is the wave number and $i^2 = -1$.

The velocity potentials φ_l ($l = D$ or $l = i$) satisfy the Laplace equation everywhere in the fluid domain. Moreover, in order to form the first-order boundary value problem, they are subjected to the following linearized boundary conditions corresponding to the combined kinematic and dynamic free-surface condition (Eq. 10), the bottom boundary condition on the assumed horizontal sea bed (Eq. 11) and the Neumann boundary conditions on the wetted surface of the bodies (Eqs. 12-13) (Lee 1995; Lee and Newman 2005):

$$\frac{\partial \varphi_l}{\partial Z} - \frac{\omega^2}{g}\varphi_l = 0 \quad \text{on} \quad Z = 0 \tag{10}$$

$$\frac{\partial \varphi_l}{\partial Z} = 0 \quad \text{on} \quad Z = -d \tag{11}$$

$$\frac{\partial \varphi_D}{\partial n} = 0 \tag{12}$$

$$\frac{\partial \varphi_i}{\partial n} = n_3^i \quad \text{for} \quad i = 1, \dots, N \tag{13}$$

In Eq. (13), n_3^i denotes the normal unit vector of PA$_i$ in the vertical direction.

Green's theorem is deployed to form the boundary integral equations for the unknown diffraction and radiation potentials on the boundaries of all bodies (PAs and wall) and of the PAs respectively. The relevant boundary value problem is, then, solved based on the three dimensional low-order panel method (Lee 1995; Lee and Newman 2005). The assumption of a wall of negligible thickness leads to the utilization of zero-thickness dipole panels (Lee and Newman 2005) for modeling its wetted surface.

Having solved the aforementioned problem, first-order hydrodynamic forcing quantities are obtained using the following equations:

$$F_3^i = -i\omega\rho \iint_{S_b^i} n_3^i \varphi_D ds\,, \qquad i = 1, \dots, N \tag{14}$$

$$A_{ij} - \frac{i}{\omega}B_{ij} = \rho \iint_{S_b^i} n_3^i \varphi_j ds\,, \quad i,j = 1, \dots, N \tag{15}$$

where, F_3^i is the heave exciting force applied on the i^{th} PA, A_{ij} and B_{ij} are the added mass and radiation damping coefficients, S_b^i is the wetted surface of the i^{th} PA and ρ is the water density.

The complex amplitudes of the PAs' heave motions, ξ_3^i, $i = 1, \dots, N$, are, then, calculated by solving the following linear system of equations:

$$\sum_{i=1}^{N}\left[-\omega^2\left(M_{ij} + A_{ij}\right) + i\omega\left(B_{ij} + B_{ij}^{PTO}\right) + C_{ij}\right]\xi_3^i = F_3^j \quad j = 1, \dots, N \tag{16}$$

In Eq. (16), M_{ij} and C_{ij} are, respectively, the mass matrix and the hydrostatic-gravitational stiffness coefficients, while B_{ij}^{PTO} are the damping coefficients originating from the PTO mechanism. For an i^{th} PA of the cluster, this mechanism is modeled as a linear damping system of constant damping coefficient b_{PTOi} (Figure 1(b)), actuated by the PA's heave motion. Accordingly, in Eq. (16), $B_{ij}^{PTO} = b_{PTOi}$ for $i = j = 1, \dots, N$, while $B_{ij}^{PTO} = 0$ for $i \neq j$. The coefficients M_{ij} for $i = j = 1, \dots, N$ are equal to ρV, where $V = 2/3\pi\alpha^2 c$ is the submerged volume of a PA, while $M_{ij} = 0$ for $i \neq j$. As for the hydrostatic-gravitational stiffness coefficients, given that each device is assumed to oscillate only in the vertical direction, $C_{ij} = 0$ for $i \neq j$, and C_{ij} for $i = j = 1, \dots, N$ are obtained as follows:

$$C_{ij} = \rho g \iint_{S_b^i} n_3^i ds\,, \quad i,j = 1, \dots, N \tag{17}$$

Having solved the equation of motion, the total averaged power, p_{tot}, absorbed by the whole cluster for specific positions of the PAs in front of the wall and for given values of ω and β, is, finally, calculated as:

$$p_{tot} = \sum_{i=1}^{N} p_i = \sum_{i=1}^{N} 0.5 b_{PTOi} \omega^2 \left|\xi_3^i\right|^2 \quad (18)$$

where p_i is the averaged power absorbed by the i^{th} PA of the cluster.

3 Examined Optimization Cases

The optimization process described above is applied for a cluster of $N = 5$ identical oblate spheroidal PAs situated at an area of water depth $d = 10$ m in front of a bottom-mounted wall of length $L_{wall} = 72$ m. The geometrical and the PTO characteristics of the PAs have been defined according to the previous works of Tzelos et al. (2020) and Loukogeorgaki et al. (2020). Specifically, each i^{th}, $i = 1, \dots, 5$, PA has radius $\alpha = 2.0$ m and draft $c = 1.7$ m, while its constant PTO damping coefficient b_{PTOi}, is selected, so that power absorption is maximized at the heave natural frequency, ω_{n3}, of a single, isolated (i.e., without the presence of the wall) device. Accordingly, b_{PTOi} is set equal to the heave radiation damping of the isolated device at $\omega = \omega_{n3}$. For the examined PA geometry, ω_{n3} is 2.4 rad/s resulting to $b_{PTOi} = 10{,}322.20$ Ns/m. The multi-body cluster and the wall are subjected to the action of perpendicular to the leeward boundary waves (i.e., $\beta = 270$ deg, Figure 1(a)).

Aiming at investigating various aspects of the examined physical problem, seven different optimization cases are formed and solved (Table 1). Optimization case C1 corresponds to a simple, single-variable constrained optimization problem, where a common for all PAs optimum perpendicular distance, Y_{com}, from the wall is being sought, assuming that the cluster has the form of a linear array. More specifically, the cluster is taken to consist of devices distributed uniformly along a line parallel to the wall at -16.0 m $\leq X \leq$ 16.0 m (i.e., $L_{edge} = 20.0$ m), with a fixed pre-defined center-to-center distance equal to 8.0 m. Accordingly, only the constraint described by Eq. (3) is taken into account, by setting $Y_i = Y_{com}$ for $i = 1, \dots, 5$. C1 is solved for perpendicular to the wall waves of $\omega = 2.4$ rad/s (i.e., equal to heave natural frequency of the isolated device), where the power absorption ability of the cluster is driven by resonance phenomena (Loukogeorgaki et al. 2020). It is noted that C1 enabled us also to assess the efficiency of the developed in the present paper optimization process, by comparing the optimum results with the parametric numerical results of Loukogeorgaki et al. (2020). Continuing with the rest optimization cases, C2a and C2b aim at investigating the effect of the incident wave frequency on the formation of the optimum layouts and on the power absorbed by the cluster. In that respect, the optimization problem of C2a is solved for $\omega = 2.4$ rad/s, while a regular wave of a smaller frequency equal to 1.1 rad/s is considered in the case of C2b. At the latter frequency, the cluster's power absorption ability is mainly driven by the positive interaction effects between the cluster and the wall (Loukogeorgaki et al. 2020). In both cases, the PAs are free to be situated along the whole wall length. Accordingly, Eq. (4) is applied for $L_{edge} = 0$ m, while the rest spatial constraints are imposed by deploying Eqs. (2) and (3). C3a and C3b are similar to C2a and C2b respectively; however, for the former optimization cases the PAs are restrained to be distributed along part of the whole wall length and, more specifically, at -16.0 m $\leq X \leq$ 16.0 m. Thus, Eq. (4) is applied with $L_{edge} = 20.0$ m. Finally, optimization cases C4a~C4b aim at determining the formation of optimum symmetrical (with respect to the global OY axis) layouts considering that the PAs can be situated respectively at -32.0 m $\leq X \leq$ 32.0 m (i.e., along the whole wall length). Accordingly, spatial constraints are imposed by deploying Eqs. (2), (3) and Eq. (5), as well as Eq. (4) with $L_{edge} = 0$ m. Case C4a is solved for $\omega = 2.4$ rad/s, while a regular wave of $\omega = 1.1$ rad/s is considered for case C4b.

Table 1 Examined optimization cases and their main characteristics.

Optimization Case	Design variables to be optimized	Imposed constraints	ω (rad/s)
C1	$Y_i = Y_{com}, i = 1, \dots, 5$	Eq. (3)	2.4
C2a	X_i and Y_i, $i = 1, \dots, 5$	Eqs. (2), (3) and (4) with $L_{edge} = 0$ m	2.4
C2b			1.1
C3a	X_i and Y_i, $i = 1, \dots, 5$	Eqs. (2), (3) and (4) with $L_{edge} = 20$ m	2.4
C3b			1.1
C4a	X_i and Y_i, $i = 1, \dots, 5$	Eqs. (2), (3), (4) with $L_{edge} = 0$ m, and Eq. (5)	2.4
C4b			1.1

For all optimization cases of Table 1, the following options were defined at the beginning of the optimization process: (a) consideration of an 0.1 m X 0.1 m grid for placing the devices (i.e., the design variables X_i and Y_i, $i = 1, \dots, 5$ have values up to their first decimal), (b) application of Eq. (7) with $\beta_{sel} = 2.0$ and (c) crossover and mutation rates equal to 85% and 30% respectively. For optimization cases C2a and C2b, characterized by a larger solution space, optimization was performed by setting the population size M equal to 30 and the maximum number of iteration cycles (stopping criterion) equal to 1000. For the rest optimization cases of Table 1, the above parameters were taken respectively equal to 10 and 100, based on appropriate relevant preliminary tests, aiming at keeping the computational effort at a reasonable level, while preserving the required numerical accuracy.

4 Results and Discussion

4.1 Optimum distance of a linear array from the wall (C1 case)

Starting with the optimization case C1 (Table 1), Figure 3(a) shows schematically the corresponding optimum layout of the PAs cluster in the $X - Y$ plane. For the specific case, where the cluster corresponds to a linear array with equally-spaced devices at fixed pre-defined positions along part of the whole wall length, maximization of the total absorbed power, p_{tot}, at $\omega = 2.4$ rad/s is achieved by placing all the PAs at a common perpendicular distance from the wall, Y_{com}, equal to 5.6 m. This outcome is in line with the parametric results of Loukogeorgaki et al. (2020). More specifically, in that investigation the effect of the distance of the aforementioned array from the wall on p_{tot} was assessed by performing a frequency-based hydrodynamic analysis for six different Y_{com} values equal to 3.0 m, 4.0 m, 5.0 m, 6.0 m, 7.0 m and 8.0 m. The corresponding results illustrated that in the frequency range 2.0 rad/s < ω < 2/5 rad/s, where resonance phenomena occur, the increase of Y_{com} up to 6.0 m, improves consecutively the array's power absorption ability, while a further increase of Y_{com} leads to a gradual decrease of p_{tot}. This in turn advocates that maximization of p_{tot} at $\omega = 2.4$ rad/s can be achieved by deploying the devices of the linear array at a perpendicular distance from the wall within 5.0 m $< Y <$ 7.0 m, as it has been illustrated from the optimum solution of C1. As for p_{tot} absorbed by the linear array placed at an optimum distance from the wall, its value was calculated equal to 389 kW/m^2. This is shown in Figure 3(b), where the total power absorbed by the optimally-arranged array at various frequencies ω is plotted.

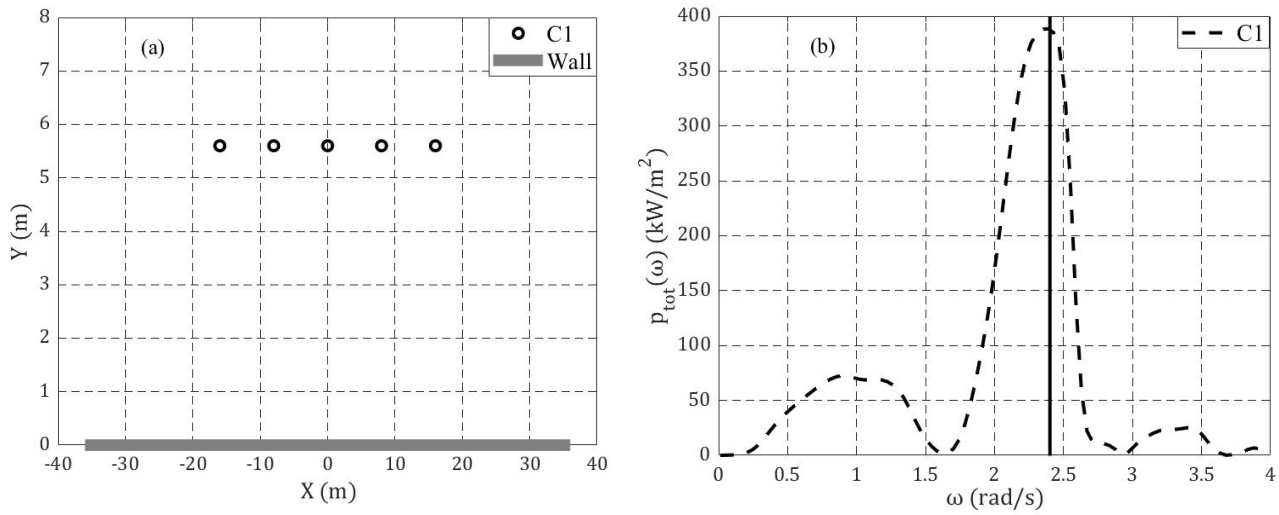

Figure 3 (a) Optimum layout of the PAs cluster in front of the wall for C1 (b): p_{tot} absorbed at various ω by the optimally-arranged array of C1 (the black vertical line denotes the frequency considered to solve the optimization problem).

4.2 Optimum layouts for different incident wave frequencies (C2a and C2b cases)

Table 2 shows the results (optimum values of the design variables X_i and Y_i, $i = 1, \dots, 5$ and maximized values of the objective function p_{tot}) for C2a and C2b (Table 1). For these cases, the optimum layouts of the PAs cluster in front of the wall in the $X - Y$ plane are shown schematically in Figure 4(a), while furthermore, Figure 4(b) includes the p_{tot} absorbed by the optimally-arranged clusters at various frequencies ($p_{tot} - \omega$ curves). It is recalled that for both C2a and C2b cases, the PAs are free to be situated along the whole wall length; however, contrary to C2a, where the optimization problem is solved for $\omega = 2.4$ rad/s, coinciding with the PA's heave natural frequency, in the case of C2b optimization is performed for a smaller ω equal to 1.1 rad/s.

The results of Table 2 and Figure 4(a) demonstrate that the optimum layout for C2a is realized by placing the devices at large perpendicular distances from the wall, with Y values ranging from 4.9 m up to 5.2 m. The latter values decrease smoothly as we are moving from the middle device (PA_3) towards each outer device (PA_1 or PA_5). This in turn leads to an Λ-shaped arrangement of the devices in front of the wall. As for the locations of the PAs along the OX axis, the devices are distributed within a large part of the total wall length (i.e., at -30 m $< X <$ 30 m) forming an almost symmetrical arrangement with respect to the OY axis. More specifically, the middle PA (PA_3) is situated very close to the middle of the wall (i.e., at $X = -0.1$ m), while PA_2 and PA_4 are placed at an almost equal along OX center-to-center distance ($\approx$ 13.6 m) from PA_3. Similar are the positions of the outer devices PA_1 and PA_5 with regard to PA_2 and PA_4 respectively; however, a larger along OX center-to-center distance ($\approx$ 14.9 m) is observed. Regarding C2b, the consideration of $\omega =$ 1.1 rad/s as the frequency for performing the optimization, introduces significant differences on the features of the cluster's optimum layout compared to C2a. More specifically, and contrary to C2a, the PAs within the optimally-arranged cluster are situated at very small perpendicular distances from the wall, with Y values ranging from 2.1 m up to 2.8 m (i.e., close to the smallest allowable perpendicular distance of 2.1 m). Furthermore, the optimum layout is characterized by the formation of two sub-clusters of two or three closely-positioned bodies situated near the two wall edges.

Table 2| Optimization results for C2a and C2b.

Case	X_1 (m)	X_2 (m)	X_3 (m)	X_4 (m)	X_5 (m)	Y_1 (m)	Y_2 (m)	Y_3 (m)	Y_4 (m)	Y_5 (m)	p_{tot} (kW/m²)*
C2a	-28.5	-13.6	-0.1	13.6	28.4	4.9	5.0	5.2	4.9	4.9	553
C2b	-26.1	-21.8	-17.7	19.9	24.2	2.8	2.1	2.3	2.3	2.1	159

* At $\omega = 2.4$ rad/s (C2a) and at $\omega = 1.1$ rad/s (C2b), where optimization is performed.

As for the averaged power absorbed by the optimally-arranged clusters, the maximized at $\omega = 2.4$ rad/s p_{tot} in the case of C2a takes the value of 553 kW/m^2 (Table 2), which represents an 42.2% increase compared to C1. This value corresponds to the global peak of the $p_{tot} - \omega$ curve (Figure 4(b)), which, furthermore, is characterized by the existence of a local peak of 92 kW/m^2 at $\omega = 1.1$ rad/s. For C2b, the p_{tot} value maximized at $\omega = 1.1$ rad/s is equal to 159 kW/m^2 (Table 2). The corresponding $p_{tot} - \omega$ curve has a total different variation pattern compared to the $p_{tot} - \omega$ curve of C2a (Figure 4(b)), characterized by the formation of a global peak ($\sim$200 kW/m^2) at $\omega = 1.5$ rad/s. Furthermore, the optimally-arranged cluster of C2b leads to a great reduction of p_{tot} in the frequency range, where resonance phenomena occur.

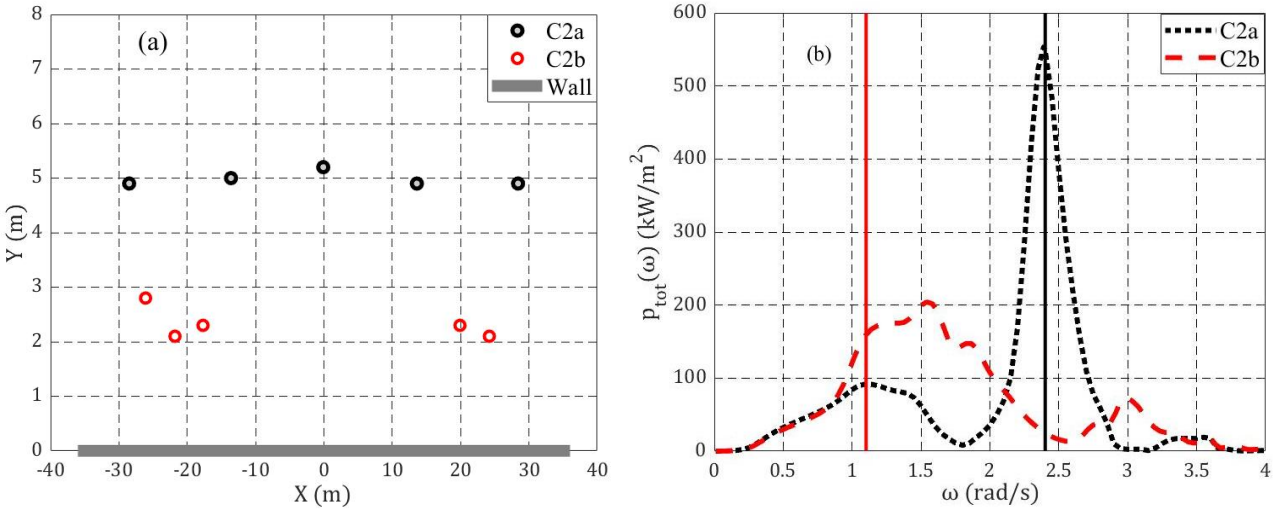

Figure 4| (a): Optimum layouts of the PAs cluster in front of the wall for C2a~C2b (b): p_{tot} absorbed at various ω by the optimally-arranged clusters of C2a~C2b (black and red vertical lines denote respectively the frequencies considered in C2a and C2b to solve the optimization problem).

4.3 Optimum layouts by deploying part of the whole wall length (C3a and C3b cases)

The optimization results (optimum values of the design variables X_i and Y_i, $i = 1, \dots, 5$ and maximized values of the objective function p_{tot}) obtained in the case of C3a and C3b (Table 1), where the PAs are restrained to be situated along a part of the whole wall length (i.e., at -16.0 m $\leq X \leq$ 16.0 m) are included in Table 3. The corresponding optimum layouts are shown schematically in Figure 5(a), where, additionally, the optimum cluster configurations of cases C2a~C2b are included for comparison purposes. Starting with C3a, where optimization is performed at $\omega = 2.4$ rad/s, the PAs within the optimally-arranged cluster are situated at larger, compared to C2a, perpendicular distances from the leeward boundary, with Y values varying between 4.7 m up to 5.7 m. Moreover, the devices are distributed along the whole allowable wall length, with the middle PA placed very close to the middle of the wall (i.e., at $X = 0.3$ m) and the two outer devices located at or close to the bounds of the allowable X solution space. PA_2 and PA_4 are situated at $X = -9.2$ m and $X = 8.7$ m respectively, leading to unequal along OX center-to-center distances between adjacent bodies, contrary to the case of C2a. As for C3b, where optimization is performed at $\omega = 1.1$ rad/s, the optimally-arranged cluster has similar features with the corresponding one of C2b. Specifically, the optimum layout has two sub-clusters of two or three closely-positioned bodies near the two edges of the allowable for deploying the PAs wall length, while the PAs are placed very close to the wall (i.e., the optimum Y values vary between 2.1 m and 2.3 m). However, it should be noted that the devices are distributed more uniformly along the OY axis compared to C2b.

Table 3 Optimization results for C3a and C3b.

Case	X_1 (m)	X_2 (m)	X_3 (m)	X_4 (m)	X_5 (m)	Y_1 (m)	Y_2 (m)	Y_3 (m)	Y_4 (m)	Y_5 (m)	p_{tot} (kW/m²)*
C3a	-15.3	-9.2	0.3	8.7	16.0	4.7	5.6	5.1	5.7	5.0	392
C3b	-15.9	-11.9	-7.4	11.8	15.8	2.3	2.1	2.3	2.2	2.1	129

* At $\omega = 2.4$ rad/s (C3a) and at $\omega = 1.1$ rad/s (C3b), where optimization is performed.

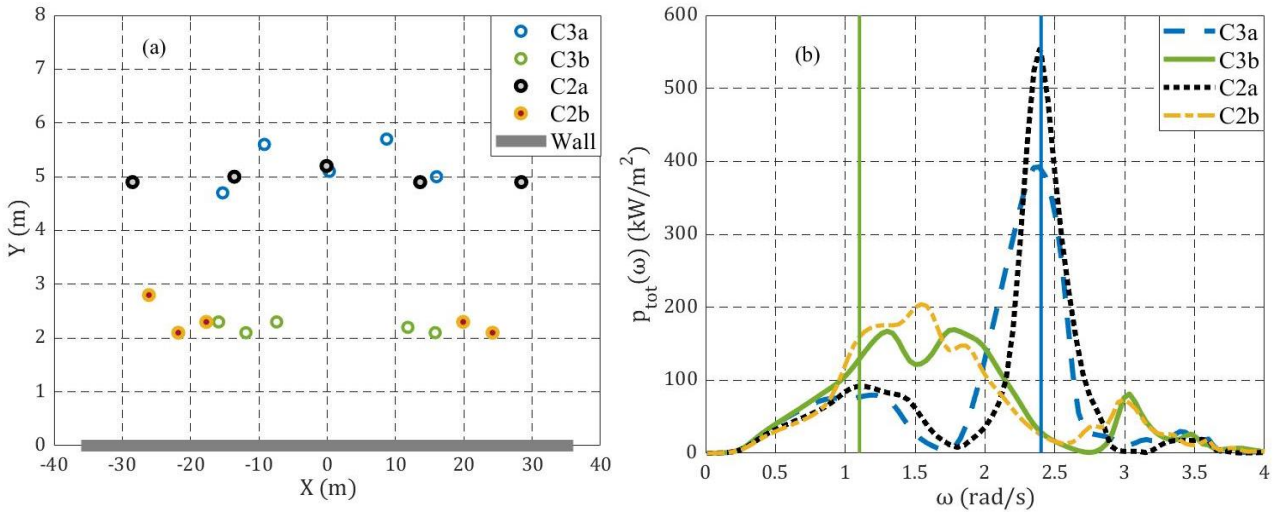

Figure 5 (a): Optimum layouts of the PAs cluster in front of the wall for C3a~C3b and C2a~C2b (b): p_{tot} absorbed at various ω by the optimally-arranged clusters of C3a~C3b and C2a~C2b (blue and green vertical lines denote respectively the frequencies considered in C3a~C2a and C3b~C2b to solve the optimization problem).

With regard to the averaged power absorbed by the optimally-arranged clusters, the p_{tot} value maximized at $\omega = 2.4$ rad/s in the case of C3a is equal to 392 kW/m^2 (Table 3) corresponding to an 29.1% decrease compared to C2a (Table 2). The $p_{tot} - \omega$ curve obtained for C3a has a similar variation pattern with the corresponding curve of C2a (Figure 5(b)); however, in the former case the p_{tot} local peak in the low frequency range occurs at $\omega = 1.2$ rad/s and has a smaller value equal to 79.5 kW/m^2. As for C3b, the maximized at $\omega = 1.1$ rad/s p_{tot} value equals 129 kW/m^2 (Table 3), representing an 18.9% decrease compared to C2b (Table 2). The corresponding $p_{tot} - \omega$ curve (Figure 5(b)) has of a global peak (~169 kW/m^2) at $\omega = 1.8$ rad/s, while, the optimum layout of C3b leads to a great reduction of p_{tot} at $\omega = 2.4$ rad/s, similarly to C2b. Based on all the above, it is straightforward that the deployment of part of the whole wall length for placing the devices reduces the power absorption ability of the optimally-arranged clusters, irrespectively of the wave frequency considered for conducting the optimization.

4.4 Optimum symmetrical layouts (C4a and C4b cases)

With regard to the cases C4a and C4b, where optimum symmetrical (with respect to the OY axis) layouts are determined by considering the whole wall length available for placing the PAs, Table 4 shows the corresponding optimization results, while Figure 6(a) depicts schematically the relevant optimally-arranged clusters in the $X - Y$ plane. In the latter figure, the optimum layouts obtained in the cases C2a~C2b are again included for comparison purposes. For C4a, where optimization is performed at $\omega = 2.4$ rad/s, the PAs of the optimally–arranged cluster are situated at large perpendicular distances from the wall, with Y values varying from 4.7 m up to 5.1 m, and they are distributed within a large part of the total wall length (i.e., at -30 m $< X <$ 30 m). Due to symmetrical considerations, the middle PA (PA$_3$) is located in the middle of the wall (i.e., $X_3 = 0.0$ m), while PA$_2$ and PA$_4$ are situated at a horizontal (along OX) center-to-center distance of 13.5 m with respect to PA$_3$. Finally, the two outer devices are located at a bit larger along OX center-to-center distance from PA$_2$ and PA$_4$ respectively, equal to 14.9 m. By comparing Tables 2 and 4 and taking into account the results of Figure 6(a), we can conclude that the optimum layouts of C4a and C2a are quite similar. However, in the case of C4a a more uniform distribution of the PAs along the OY axis is observed contrary to C2a. Regarding C4b, where optimization is performed at $\omega = 1.1$ rad/s, the optimum layout is realized by placing all the PAs along a straight, parallel to the leeward boundary, line at $Y = 2.1$ m (i.e., at the smallest allowable perpendicular distance from the wall). This feature is not observed in the case of C2b (Table 2, Figure 6(a)). Furthermore, PA$_3$ is located in the middle of the wall (i.e., $X_3 = 0.0$ m), due to symmetrical considerations, resulting to the formation of two sub-clusters of two, contrary to C2b, closely-positioned bodies near the two wall edges.

Table 4 Optimization results for C4a and C4b.

Case	X_1 (m)	X_2 (m)	X_3 (m)	X_4 (m)	X_5 (m)	Y_1 (m)	Y_2 (m)	Y_3 (m)	Y_4 (m)	Y_5 (m)	p_{tot} (kW/m²)*
C4a	-28.4	-13.5	0.0	13.5	28.4	4.7	5.0	5.1	5.0	4.7	551
C4b	-21.5	-17.3	0.0	17.3	21.5	2.1	2.1	2.1	2.1	2.1	147

* At $\omega = 2.4$ rad/s (C4a) and at $\omega = 1.1$ rad/s (C4b), where optimization is performed.

As for the total power absorbed by the optimally-arranged PAs clusters, the maximized at $\omega = 2.4$ rad/s p_{tot} for C4a takes the value of 551 kW/m^2 (Table 4), corresponding to a very small decrease (0.4%) compared to C2a (Table 2). This is attributed to the formation of very similar optimum layouts in these two optimization cases. Accordingly, the $p_{tot} - \omega$ curve obtained for C4a has the same variation pattern with the corresponding curve of C2a (Figure 6(b)) and it is characterized by the existence of a local peak of 93 kW/m^2 at $\omega = 1.1$ rad/s. Regarding C4b, the p_{tot} value maximized at $\omega = 1.1$ rad/s is obtained equal to 147 kW/m^2 (Table 4) leading to a small decrease (7.5%) compared to C2b (Table 2). The $p_{tot} - \omega$ curve of C4b (Figure 6(b)) has a global peak (~216 kW/m^2) at $\omega = 1.6$ rad/s, while, it shows significantly reduced p_{tot} values at 2.3 rad/s $< \omega <$ 2.5 rad/s, where resonance phenomena occur, similarly to C2b. However, in this frequency range the power absorption ability of the optimally-arranged cluster is a bit improved compared to C2b. Based on all the above, we can conclude that under the action of perpendicular to the wall waves, the consideration of symmetrical features in the formation of the optimum layouts reduces at a small degree the maximum power absorption ability of the optimally-arranged clusters, especially when optimization is performed at the high frequency of 2.4 rad/s.

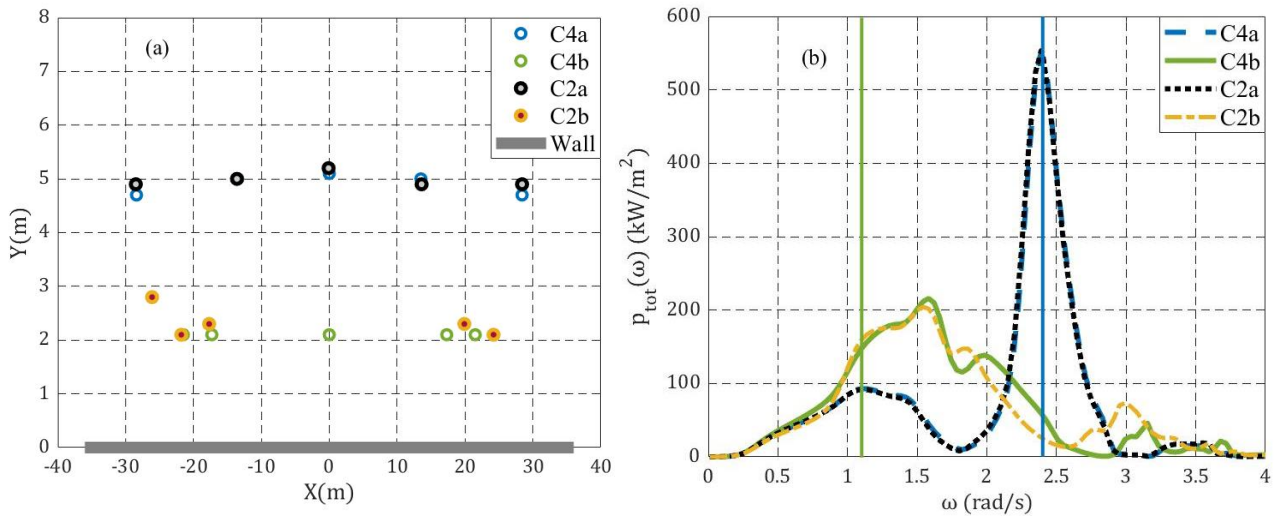

Figure 6| (a): Optimum layouts of the PAs cluster in front of the wall for C4a~C4b and C2a~C2b (b): p_{tot} absorbed at various ω by the optimally-arranged clusters of C4a~C4b and C2a~C2b (blue and green vertical lines denote respectively the frequencies considered in C4a~C2a and C4b~C2b to solve the optimization problem).

5 Conclusions

In this paper, we developed a GA-driven optimization process to determine optimum layouts of a cluster of heaving PAs in front of a bottom-mounted finite-length vertical wall under the action of regular waves. Optimum layouts maximize the averaged power absorbed by the cluster, p_{tot}, for a specific incident wave frequency and direction, while satisfying spatial constraints. Optimization is performed for a cluster of five identical semi-immersed oblate spheroidal devices subjected to perpendicular with respect to the wall waves. Initially, the optimum distance of the PAs from the wall was determined assuming that the cluster has the form of a linear array situated parallel to the leeward boundary. The relevant optimization solution was in line with the parametric numerical results of Loukogeorgaki et al. (2020), demonstrating the ability of the developed optimization process to solve efficiently the relevant problem. Next, six different optimization cases were formed and solved, aiming at investigating various aspects of the examined physical problem.

The results illustrated that for all cases examined, the incident wave frequency, ω, where optimization is performed, affects significantly the formation of the optimum layouts and the power absorption ability of the clusters. Specifically, when maximization of p_{tot} at the low frequency of 1.1 rad/s is sought, the devices within the optimally-arranged clusters are situated at very small perpendicular distances from the wall, having values equal to or very close to the lowest allowable relevant bound of $1.1a$. Furthermore, optimum layouts are characterized by the formation of a sub-cluster of closely-positioned devices near each edge of the allowable for deploying the PAs wall length. Contrary to the above, maximization of p_{tot} at the high frequency of 2.4 rad/s, coinciding with the PA's heave natural frequency, is achieved by placing the PAs at large perpendicular distances from the wall, with values varying between $2.4a$ and $2.9a$, while the optimally-arranged clusters do not show any sub-clustering feature. As for the total power absorbed by the optimally-arranged clusters, p_{tot} maximized at $\omega = 1.1$ rad/s has values $\sim 3-3.5$ times smaller compared to those maximized at $\omega = 2.4$ rad/s, since in the latter case the power absorption ability of the cluster is driven by resonance phenomena. The realization of optimum layouts very close to the leeward boundary for $\omega = 1.1$ rad/s leads also to a great reduction of p_{tot} in the frequency range, where resonance phenomena occur, and, thus, it bounds the clusters' power absorption ability at low wave frequencies.

The length of the wall considered available for placing the devices affects directly the formation of the optimum layouts, especially in the case of $\omega = 2.4$ rad/s. Specifically, when the PAs are free to be distributed along the whole available wall length, the devices within the optimum layout are located almost symmetrically with respect to the OY axis in an Λ-shaped arrangement. All these features vanish, when the PAs are restrained to be situated along part of the whole wall length, since a more random positioning of the devices within the corresponding optimum layout is observed. As for the absorbed power, the deployment of part of the whole wall length for placing the PAs reduces the power absorption ability of the optimally-arranged clusters for both examined wave frequencies. More specifically, an 29.1% and 18.9% reduction of p_{tot} maximized respectively at $\omega = 2.4$ rad/s and $\omega = 1.1$ rad/s is observed, compared to the cases, where no wall-length restrictions are taken into account.

Finally, the consideration of symmetrical with respect to the OY axis features in the formation of the optimum layouts reduces at a small degree the maximum power absorption ability of the optimally-arranged clusters, especially when optimization is performed at the high frequency of 2.4 rad/s. This is attributed to the fact that the symmetrical optimum layouts show small differences compared to those optimized without considering any symmetrical spatial restrictions. Accordingly, if the wall is oriented perpendicularly to the most predominant wave direction, optimum layouts could be determined with much less computational effort by exploiting symmetrical features.

The present work could be further deployed in order to assess the effect of the devices' geometrical characteristics and/or of the stiffness resulting from the configurations attaching the PAs on the wall on the formation of the optimum layouts and the maximized absorbed power. Moreover, optimization could be performed by including in the hydrodynamic analysis nonlinear and/or viscous effects. Finally, the determination of optimally-arranged PAs under oblique waves and in front of a parabolic-shaped wall could also present items for future investigation.

Author contributions (CRediT)

RI: Conceptualization, Methodology, Investigation, Software, Formal Analysis, Writing-original draft. EL: Conceptualization, Methodology, Investigation, Supervision, Writing-review & editing.

Notations

Name	Symbol	Unit
Number of Point Absorbers (PAs) in the cluster	N	-
i^{th} $(i = 1, \dots, N)$ PA of the cluster	i	-
Wall length	L_{wall}	m
Water depth	d	m
Radius of the oblate spheroidal PA	α	m
Draft of the oblate spheroidal PA	c	m
Damping coefficient of the PTO mechanism of the i^{th} PA	b_{PTOi}	Ns/m
X, Y spatial coordinates of i^{th} PA center in the global $OXYZ$ coordinate system	X_i, Y_i	m
Horizontal (along OX) distance of the two outer PAs from the wall edges	L_{edge}	m
Wave frequency	ω	rad/s
Wave angle	β	deg
Population of chromosomes	M	-
m^{th} $(m = 1, \dots, M)$ chromosome of the population	m	-
Selection probability of the m^{th} chromosome	PS_m	-
Rank value of the m^{th} chromosome	$rank_m$	-
Selective pressures	a_{sel}, β_{sel}	-
Incident wave potential	φ_I	m^2/s
Scattered potential	φ_S	m^2/s
Diffraction potential	φ_D	m^2/s
Radiation potential associated with the i^{th} PA	φ_i	m^2/s
Velocity potential ($l = D$ or $l = i$)	φ_l	m^2/s
Complex amplitude of the heave motion of the i^{th} PA	ξ_3^i	m
Normal unit vector of the i^{th} PA in the vertical direction	n_3^i	-
Gravitational acceleration	g	m/s^2
Wave amplitude	A	m
Wave number	k	m^{-1}
Heave exciting force of the i^{th} PA	F_3^i	N
Mass matrix coefficients	M_{ij}	kg
Added mass matrix coefficients	A_{ij}	kg
Radiation damping matrix coefficients	B_{ij}	Ns/m
Damping coefficients originating from the PTO mechanism	B_{ij}^{PTO}	Ns/m
Hydrostatic-gravitational stiffness matrix coefficients	C_{ij}	N/m
Wetted surface of the i^{th} PA	S_b^i	m^2
Water density	ρ	kg/m^3
Submerged volume of a PA	V	m^3
Total averaged power absorbed by the whole cluster	p_{tot}	kW/m^2
Averaged power absorbed by the i^{th} PA	p_i	kW/m^2

References

Astariz, S.; Vazquez, A.; Iglesias, G. (2015): Evaluation and comparison of the levelized cost of tidal, wave, and offshore wind energy. In: Journal of Renewable and Sustainable Energy 7 (5), paper No. 53112.

Child, B. F. M.; Venugopal, V. (2010): Optimal configurations of wave energy device arrays. In: Ocean Engineering 37(16), 1402–1417.

Davis L. (1991): Handbook of genetic algorithms. Van Nostrand Reinhold, New York (385).

Exxon Mobil Corporation (2019): 2019 Outlook for energy: A perspective to 2040 (58).

Fang, H. W.; Feng, Y. Z.; Li, G. P. (2018): Optimization of wave energy converter arrays by an improved differential evolution algorithm. In: Energies 11, paper No. 3522.

Giassi, M.; Göteman, M. (2018): Layout design of wave energy parks by a genetic algorithm. In: Ocean Engineering 154, 252–261.

Gkaraklova, S.; Chotzoglou, P.; Loukogeorgaki, E. (2021): Frequency-based performance analysis of an array of wave energy converters around a hybrid wind–wave monopile support structure. In: Journal of Marine Science and Engineering 9 (1), paper No. 2.

Gwiazda, T. D. (2006): Genetic algorithms reference: Volume I Crossover for single-objective numerical optimization problems. Tomaszgwiazda e-books, Lomianki (412).

Haq, E.; Ahmad, I.; Abid H.; Ibrahim A. M. (2019): A novel selection approach for genetic algorithms for global optimization of multimodal continuous functions. In: Computational intelligence and neuroscience 2019, paper No. 8640218.

Konispoliatis, D. N.; Mavrakos, S. A. (2020): Wave power absorption by arrays of wave energy converters in front of a vertical breakwater: A theoretical study. In: Energies 13 (8), paper No. 1985.

Konispoliatis, D. N.; Mavrakos, S. A.; Katsaounis, G. M. (2020): Theoretical evaluation of the hydrodynamic characteristics of arrays of vertical axisymmetric floaters of arbitrary shape in front of a vertical breakwater. In: Journal of Marine Science and Engineering 8 (1), paper No. 62.

Kumar, P.; Gospodaric, D.; Bauer, P. (2007): Improved genetic algorithm inspired by biological evolution. In: Soft Computing 11 (10), 923–941.

Lee, C. H. (1995): WAMIT theory manual. MIT Report 95-2, Department of Ocean Engineering, MIT (66).

Lee, C. H.; Newman, J. N. (2005): Computation of wave effects using the panel method. In: Numerical Models in Fluid-Structure Interaction (Chakrabarti S, editor), WIT Press, 211–251.

López, I.; Andreu, J.; Ceballos, S.; Martínez de Alegría, I.; Kortabarria, I. (2013): Review of wave energy technologies and the necessary power-equipment. In: Renewable and Sustainable Energy Reviews 27, 413–434.

Loukogeorgaki, E.; Boufidi, I.; Chatjigeorgiou, I. K. (2020): Performance of an array of oblate spheroidal heaving wave energy converters in front of a wall. In: Water 12 (1), paper No. 188.

Loukogeorgaki, E.; Chatjigeorgiou, I. K. (2019): Hydrodynamic performance of an array of wave energy converters in front of a vertical wall. In: Proceedings of the 13th European Wave and Tidal Energy Conference (EWTEC 2019). Napoli, Italy, paper No. 1464.

Loukogeorgaki, E.; Michailides, C.; Lavidas, G.; Chatjigeorgiou I. K. (2021): Optimum layouts of a cluster of heaving point absorbers in front of a wall. In: Proceedings 31st International Offshore and Polar Engineering Conference (ISOPE), Rhodes (virtual/online), 1, 736–743.

McGuinness, J.; Thomas, G. (2016): Hydrodynamic optimisation of small arrays of heaving point absorbers. In: Journal of Ocean Engineering and Marine Energy 2, 439–457.

Neshat, M.; Abbasnejad, E.; Shi, Q.; Alexander, B.; Wagner, M. (2019): Adaptive neuro-surrogate-based optimisation method for wave energy converters placement optimization. In: Processding International Conference on Neural Information Processing (ICONIP 2019), Sydney, 353–366.

Oyama, A.; Obayashi, S.; Nakahashi, K. (2000): Real-coded adaptive range genetic algorithm and its application to aerodynamic design 43 (2), 124–129.

Raftery, A. E.; Zimmer, A.; Frierson, D. M. W.; Startz, R.; Liu, P. (2017): Less than 2 °C warming by 2100 unlikely. In: Nature Climate Change 7, 637–641.

Razali, N. M.; Geraghty, J. (2011): Genetic algorithm performance with different selection strategies in solving TSP. In: Proceedings of the World Congress on Engineering 2011, London, II, 1134–1139.

Ruiz, P. M.; Nava, V.; Topper, M. B. R.; Minguela, P. R.; Ferri, F.; Kofoed, J. P (2017): Layout optimisation of wave energy converter arrays. In: Energies 10(9), paper No. 1262.

Rusu, E.; Onea, F. (2018): A review of the technologies for wave energy extraction. In: Clean Energy 2(1), 10–19.

Sharp, C.; DuPont, B. (2018): Wave energy converter array optimization: A genetic algorithm approach and minimum separation distance study. In: Ocean Engineering 163, 148–156.

Shopova, E. G.; Vaklieva-Bancheva, N. G. (2006): BASIC—A genetic algorithm for engineering problems solution. In: Computers & Chemical Engineering 30 (8), 1293–1309.

The MathWorks, Inc. (2019): MATLAB, Version 9.6 (2019a). Natick, Massachusetts, United States.

Tzellos, N.; Loukogeorgaki, E.; Anastasiou, E.; Chatjigeorgiou, I. K. (2020).: Performance of an oblate spheroidal heaving wave energy converter. In: Proceedings 30th International Offshore and Polar Engineering Conference (ISOPE), Shanghai (online), 1, 116–123.